DA-NN: A ResNet-Based Architecture with Domain Adaptation for Automatic EEG Artifact Identification

Emmanuel de Jesús Velásquez-Martínez[1][a] Miguel Ángel Porta-García[1][b]
[1]*Centro de Investigación e Innovación en Tecnologías de la Información y Comunicación (INFOTEC), Ciudad de México 14050, México*
iemmanuelvm@gmail.com, miguel.porta@infotec.mx

Keywords: Artifact Identification, Domain Adaptation, Semi-Supervised Deep Learning.

Abstract: Electroencephalography (EEG) is a fundamental tool for studying brain activity; however, EEG signals are frequently contaminated by physiological and non-physiological artifacts that affect interpretation and diagnostic accuracy. Accurate artifact classification during preprocessing is therefore essential for reliable EEG analysis. While this problem has been addressed using both traditional and deep learning methods, many deep learning models rely on either synthetic data or real expert-labeled datasets and often exhibit degraded performance when evaluated on data differing from the training set, indicating limited generalization due to insufficient domain adaptation. To address this limitation, this study proposes a Domain Adaptation Neural Network (DA-NN) that generalizes EEG artifact identification across synthetic and real signals. The proposed semi-supervised architecture reduces the domain gap and achieves robust performance, reaching 91.59% classification accuracy.

1 INTRODUCTION

Electroencephalography (EEG) is widely used in clinical and neuroscience research due to its ability to provide direct, non-invasive measurements of brain activity with high temporal resolution (Huang et al., 2024). It plays a key role in the diagnosis, monitoring, and prognosis of neurological disorders (Saba-Sadiya et al., 2021), as well as in the development of brain–computer interfaces (BCI) (Chuang et al., 2022). EEG signals are recorded using scalp electrodes positioned according to the international 10–20 system, covering frontal, occipital, temporal, and parietal regions (Jackson and Bolger, 2014). These signals reflect electrical voltages generated by synchronous neuronal activity (Ahmed, 2022); however, their low amplitude makes them highly susceptible to external interference. Such interferences, known as artifacts, are non-cerebral signals classified as physiological or non-physiological according to their origin (Quintero-Rincón et al., 2021), and can compromise data analysis and diagnostic accuracy (Cai et al., 2025).

Figure 1 illustrates representative artifact types from the Temple University Hospital EEG dataset (TUH-EEG) (Hamid et al., 2020), including eye movement, muscle activity, shivering, chewing, and electrode pop artifacts. These distortions typically manifest as abrupt changes in amplitude and frequency, making reliable brain-signal analysis challenging.

Recent literature on EEG artifact treatment mainly groups methods into two approaches: classification and elimination. Classification methods aim to identify the type of interference in the signal to enable the application of specific correction strategies. Representative works include (Kim and Keene, 2019; **?**; **?**; **?**), employing convolutional neural networks (CNNs), long short-term memory (LSTM) networks, Transformers, and hybrid architectures. In contrast, artifact elimination methods directly suppress interference while preserving underlying neural activity. Recent approaches (Mashhadi et al., 2020; **?**; **?**; **?**; **?**; **?**; **?**; **?**) explore CNNs, autoencoders, U-Net architectures, Transformers, diffusion models, and hybrid methods, achieving notable improvements in RRMSE, CC, and SNR.

Despite these advances, many deep-learning–based preprocessing models adopt a one-size-fits-all assumption, presuming uniform artifact characteristics across subjects (Saba-Sadiya

[a] https://orcid.org/0009-0008-7500-3579
[b] https://orcid.org/0000-0002-7524-5833

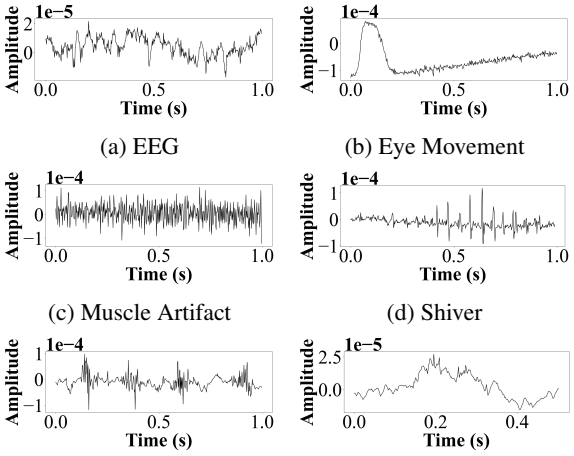

(a) EEG (b) Eye Movement

(c) Muscle Artifact (d) Shiver

(e) Chewing (f) Electrode Pop

Figure 1: Class examples for EEG artifact identification.

et al., 2021). This limits generalization, as EEG signals exhibit substantial inter- and intra-individual variability (Maiwald et al., 2023), leading to performance degradation when models are applied to data distributions different from those seen during training. Recent studies therefore emphasize the need for approaches that balance artifact handling with preservation of relevant neural information and generalize across domains (Choi, 2025; **?**).

In this work, we propose a deep-learning model, termed the Domain Adaptation Neural Network (DA-NN), which incorporates semi-supervised domain-adaptation mechanisms to improve generalization in EEG artifact classification. Unlike conventional approaches, the method leverages both real and synthetic data to capture a wider range of artifact patterns. During domain-adaptation training, only source-domain labels are used, while unlabeled target-domain data are projected into a shared latent space. A Sinkhorn loss is applied to align domain distributions, reducing discrepancy and enhancing robustness without extensive fine-tuning for new datasets (Geuter et al., 2025; **?**).

The remainder of this paper is organized as follows: Section 2 reviews related work; Section 3 describes the materials and methods; Section 4 presents the Sinkhorn-based domain-alignment process; Section 5 reports the experimental results; and Section 6 concludes the paper.

2 RELATED WORKS

This section reviews studies proposing classification strategies for EEG artifact detection. Several works rely on the TUH-EEG Corpus (Hamid et al., 2020) as a benchmark dataset, while others employ alternative datasets. In (Peh et al., 2022), a CNN–Transformer architecture with channel-wise detectors using statistical features achieved a balanced accuracy of 0.804 on TUH-EEG data. Subsequently, (Kim and Keene, 2019) introduced a lightweight CNN–LSTM model for classifying five artifact types from one-second EEG segments, reaching 67.59% accuracy and enabling real-time inference. An alternative signal representation was explored in (Maiwald et al., 2023), where EEG signals were transformed into temporal images, with Xception and EfficientNetB0 achieving F1-scores above 89%. Beyond TUH-EEG–based studies, (Bahador et al., 2020) proposed a CNN mapping multichannel EEG into a two-dimensional RGB space using Oulu University Hospital data, achieving 92.30% accuracy and an AUC of 0.96. Additionally, (Saba-Sadiya et al., 2021) introduced an unsupervised encoder–decoder model using complexity and connectivity features, achieving a Cohen's kappa of approximately 0.49.

3 MATERIALS AND METHODS

This section presents the proposed methodology to address the adaptation problem in the DA-NN model. A domain-adaptation scheme is developed between real EEG artifacts and synthetically generated artifacts to improve performance in artifact-classification tasks. The experimental procedure is organized into sequential methodological modules forming a data-processing pipeline, as illustrated in Figure 2.

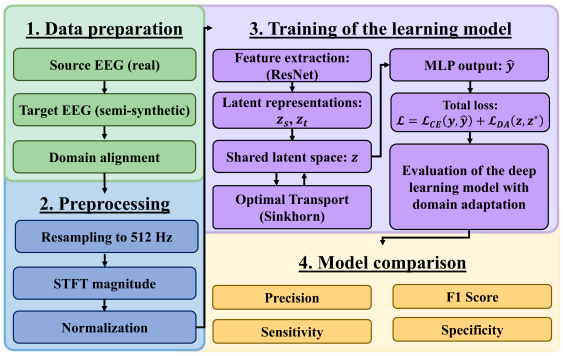

Figure 2: Proposed methodology for EEG artifact identification.

3.1 Data Preparation

Block 1 in Figure 2 corresponds to the data preparation stage. Real EEG recordings from the TUH-EEG dataset are used as the source domain, including muscle artifacts (51,052 events), ocular movements (38,569), chewing artifacts (6,482), baseline electrical potentials (172), and shivering (613). These events exhibit varying temporal durations, enabling the capture of artifact-specific variability. To address the pronounced class imbalance, majority classes were downsampled using minority classes as reference, and class weights based on inverse class frequencies were incorporated into the cross-entropy loss to penalize misclassification of underrepresented artifacts, promoting balanced learning.

Synthetic data from EEGdenoiseNet (Zhang et al., 2021) are used as the target domain to increase model variability. The dataset includes 4,514 clean EEG segments, along with 3,400 ocular and 5,598 muscle artifact segments, enabling controlled SNR conditions and standardized comparison. Since EEGdenoiseNet contains only muscle and ocular artifacts, longer-duration events from the source domain were used to synthesize missing artifact types while avoiding domain mixing. For muscle and ocular artifacts, sample counts were matched to those in EEGdenoiseNet to balance class distributions. The same downsampling and class-weighting strategy was applied across both domains to ensure comparable class priors.

Synthetic data were generated using artifact-free EEG segments from EEGdenoiseNet as baselines. Artifact segments from both datasets were added using a controlled noise-addition algorithm (Algorithm 1), which estimates clean-signal power, computes target artifact power for a given SNR, normalizes and scales the artifact, and performs linear summation. An SNR range from –5 dB to 5 dB was used to generate variable training data. Finally, both datasets were split into 80% for training and 20% for testing.

Data: $x(n)$: clean EEG signal, $a(n)$: artifact signal, SNR: desired SNR (dB)
Result: $y(n)$: artifact-contaminated EEG signal

Estimate clean EEG power: $\mathcal{P}_x = \frac{1}{N}\sum_{n=1}^{N} x(n)^2$
Compute target artifact power from SNR: $\mathcal{P}_a = \frac{\mathcal{P}_x}{10^{\mathrm{SNR}/10}}$
Normalize artifact to zero-mean and unit variance: $\tilde{a}(n) = \frac{a(n)-\mu_a}{\sigma_a}$
Scale artifact to desired power: $a_s(n) = \sqrt{\mathcal{P}_a}\cdot\tilde{a}(n)$
Generate synthetic contaminated EEG: $y(n) = x(n) + a_s(n)$

Algorithm 1: Synthetic addition of artifacts into EEG signals

3.2 Preprocessing

Block 2 in Figure 2 standardizes the sampling frequency of the TUH-EEG and EEGdenoiseNet datasets to 512 Hz and extracts input features for domain-adaptive deep learning models. For artifact classification, the Short-Time Fourier Transform (STFT) is applied, as defined in (1), to extract frequency information from EEG signals (Goyal and Pabla, 2015). In this formulation, $x(\cdot)$ denotes the input signal, $w(k)$ the analysis window, H the hop size, K the FFT size, m the time-frame index, k the sample index, and ω the frequency bin index. The resulting time–frequency representation enables identification of artifact-related patterns, and the magnitude spectrum is used as input to the classification model. Spectrum-based features were selected due to their reduced performance bias, as reported in (Maiwald et al., 2023). The STFT configuration uses a 512-sample window, a 60-sample hop, an analysis length of 128 samples, and a Hamming window. Finally, normalization is applied to all features used for classification to ensure stable and consistent training.

$$X(\omega, m) = \sum_{k=0}^{K-1} x(mH+k)\, w(k)\, e^{-j2\pi\omega k/K} \quad (1)$$

3.3 Training of the learning model

Block 3 in Figure 2 corresponds to the training stage of the proposed DA-NN model, including feature extraction, domain alignment, and supervised optimization. A ResNet architecture is first used to extract latent representations from the source and target domains, denoted as z_s and z_t, which are projected into a shared latent space. Domain alignment is achieved using an Optimal Transport–based approach, specifically the Sinkhorn algorithm, which minimizes divergence between distributions to obtain a joint representation. The shared latent representation z is then processed by a multilayer neural network to produce the model output $\hat{y}$.

Training optimizes a composite loss consisting

of a cross-entropy classification loss $\mathcal{L}CE(y,\hat{y})$ and a domain-adaptation loss $\mathcal{L}DA(z,z^*)$ that penalizes discrepancies between source and target latent spaces. Model performance during training is monitored using accuracy. To evaluate domain alignment, the Kullback–Leibler (KL) divergence (Shlens, 2014), Jensen–Shannon (JS) divergence (Fuglede and Topsoe, 2004), and Jensen–Shannon distance (Zunino et al., 2022) are computed, verifying the reduction of the domain gap.

3.4 Model comparison

Block 4 of Figure 2 evaluates the performance of the DA-NN model for categorical EEG artifact classification. Performance is assessed using standard metrics (Grandini et al., 2020), (Tohka and van Gils, 2021), (Géron, 2019), including precision, sensitivity, specificity, and F1-score, which together provide a comprehensive evaluation of classification effectiveness.

4 SINKHORN-BASED DOMAIN ALIGNMENT PROCESS APPLIED TO DEEP LEARNING MODELS

Domain adaptation seeks to improve target-model performance when annotated data are scarce or unavailable by leveraging knowledge from a related labeled source domain (Farahani et al., 2021), (Courty et al., 2017a). The algorithm presented in Algorithm 2 builds upon prior work (Courty et al., 2017b), (Lin et al., 2021), (Feydy et al., 2019) and is designed to train deep neural networks that extract meaningful latent representations while enhancing robustness under distributional shifts. Domain adaptation methods aim to align latent distributions learned from source and target domains when covariate shift exists (Courty et al., 2017a). In this semi-supervised setting, only source-domain labels are used for supervised learning, typically via cross-entropy loss, while adaptation is achieved by extracting latent vectors and minimizing the Sinkhorn divergence (Feydy et al., 2019). The Sinkhorn algorithm is an iterative method for solving regularized optimal transport problems by estimating a transport matrix that aligns distributions under cost and normalization constraints (Geuter et al., 2025). By minimizing the statistical distance between latent distributions, the adaptation process reduces domain discrepancy during training.

The process of Algorithm 2 (see Figure 3) begins

Data: x_s: Source domain inputs, y_s: Source domain labels, x_t: Target domain inputs, n: Batch size per domain, λ_{DA}: Weight of domain loss
Result: Model adapted to the target domain
while *not converged* **do**
  $X \leftarrow [x_s, x_t]$;
  $Y, Z \leftarrow \text{model}(X)$;
  $y_s \leftarrow Y$;
  $z_s, z_t \leftarrow Z$;
  $\mathcal{L}_{DA} \leftarrow \text{Sinkhorn}(z_s, z_t, \|z_{si} - z^*_{tj}\|_2, \varepsilon)$;
  $\mathcal{L}_{task} \leftarrow \begin{cases} \mathcal{L}_{CE}(y_s, \hat{y}_s), & \text{classification}; \end{cases}$
  $\mathcal{L} \leftarrow \mathcal{L}_{task} + \lambda_{DA} \cdot \mathcal{L}_{DA}$;
  `loss.backward();`
  `optimizer;`
end

Algorithm 2: Domain adaptation for classification tasks using Sinkhorn loss in the DA-NN model (Feydy et al., 2019)

by jointly considering the source and target feature matrices, x_s and x_t, denoted as $X = x_s, x_t$. The DA-NN model then generates predictions for both domains, $y_s, y_t \leftarrow Y$. Latent representations $z_s, z_t \leftarrow Z$ are extracted from an intermediate fully connected layer to enable domain alignment. Euclidean distances between these latent vectors are computed and used within the Sinkhorn function to estimate the minimal transport cost between the source and target distributions, aligning them during training (Feydy et al., 2019). The domain-adaptation loss is then combined with the task-specific prediction loss, and the resulting total loss is used to compute gradients and update the model parameters.

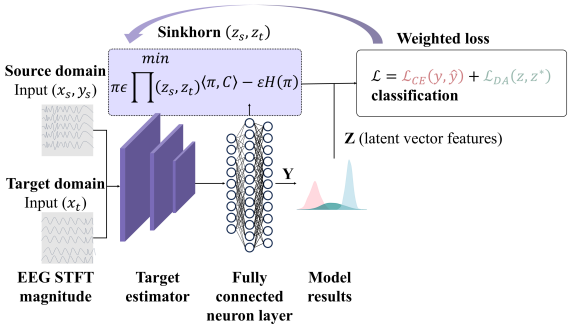

Figure 3: Neural network architecture with domain adaptation (DA-NN).

Table 1: Network architecture of the proposed DA-NN (2D-ResNet configuration 2-2-2-2).

Stage	Description	Output Shape	Params
Input	–	$(B,1,65,9)$	–
Conv1	7×7 conv, 64 ch, stride 2, pad 3; BN, ReLU	$(B,64,112,112)$	3,328
MaxPool	3×3 max pool, stride 2, pad 1	$(B,64,56,56)$	0
Layer 0	$2\times$ ResidualBlock $(64\to64)$	$(B,64,56,56)$	148,224
Layer 1	$(64\to128)$ stride 2 + downsample; $(128\to128)$	$(B,128,28,28)$	526,208
Layer 2	$(128\to256)$ stride 2 + downsample; $(256\to256)$	$(B,256,14,14)$	2,100,992
Layer 3	$(256\to512)$ stride 2 + downsample; $(512\to512)$	$(B,512,7,7)$	8,396,288
Global AvgPool	Adaptive average pooling	$(B,512,1,1)$	0
Flatten	–	$(B,512)$	0
Fully Connected	Linear $(512\to6)$	$(B,6)$	3,078
Total params			**11,178,118**
Trainable params			**11,178,118**

5 EXPERIMENTATION

This section presents the experimental results of the DA-NN model for EEG artifact classification under a domain-adaptation setting.

5.1 Neural network architecture

For EEG artifact classification, the proposed DA-NN model is based on a two-dimensional residual network (2D-ResNet) with a 2-2-2-2 configuration, tailored for time–frequency representations (Table 1) and motivated by (Maiwald et al., 2023). The network processes single-channel inputs of size $1\times65\times9$. It begins with a 7×7 convolution (64 filters, stride 2), followed by batch normalization, ReLU activation, and a 3×3 max-pooling layer. Four residual stages, each comprising two basic blocks, follow: the first preserves channel dimensionality $(64\to64)$, while subsequent stages increase filters to 128, 256, and 512, with spatial downsampling via stride 2. Global average pooling precedes a fully connected layer producing logits for six classes. The architecture contains 11.18,M trainable parameters.

Training follows the domain-adaptation scheme described in Algorithm 2 and Figure 3, using labeled source-domain data and both labeled and unlabeled target-domain samples. The model was trained for 100 epochs with the Adam optimizer (learning rate 1×10^{-3}, weight decay 1×10^{-10}), minimizing cross-entropy loss on the source domain with an additional Sinkhorn-based regularization term. Gradient clipping with a threshold of 1.0 was applied to improve numerical stability.

5.2 Learning behavior of the neural network

Figure 4 presents the accuracy metric behavior of the DA-NN model, applied to the artifact classification task under the domain adaptation approach. The accuracy curve corresponding to the source domain during training, represented with blue markers, reaches an average value close to 97.96%, indicating that the model effectively learns from these data. In contrast, the curve associated with the target domain during training, shown in orange, achieves an average accuracy of approximately 92.17%. For the source domain test data, represented by the green line, the curve stabilizes at an average of 89.34%, while for the target domain test set, represented by the red line, an average accuracy of 91.04% is obtained.

On the other hand, the markers below 70% correspond to the results in the target domain without applying the domain adaptation algorithm (see Algorithm 2) to the learning model. This behavior demonstrates that when the model performs inference on a dataset different from the one used during training and no domain adaptation is applied, its performance tends to decrease. This effect is associated with the lack of variability in the training data, resulting in an average accuracy of 67%.

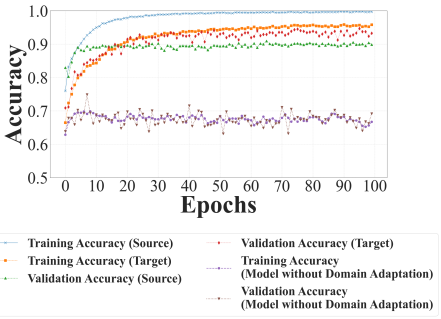

Figure 4: Training and validation accuracy over epochs.

Another metric used to assess the DA-NN domain-adaptation mechanism consists of three divergence measures (Figure 5). The Jensen–Shannon divergence (green line), its scaled variant (orange line), and the Kullback–Leibler divergence (blue line) exhibit a progressive reduction across training epochs, indicating increasing alignment between the latent distributions of the source and target domains. This trend demonstrates that the model effectively learns shared representations, enabling artifact classification in both real and synthetic EEG data.

5.3 Results of artifact classification in EEG on the validation set

The performance of the DA-NN model was evaluated using a normalized confusion matrix (Figure 6), which summarizes correct and incorrect predictions for each class. The model distinguishes five artifact types—Chewing, Electrode Pop, Eye Movement, Muscle, and Shiver—as well as clean EEG activity. High classification performance is observed across

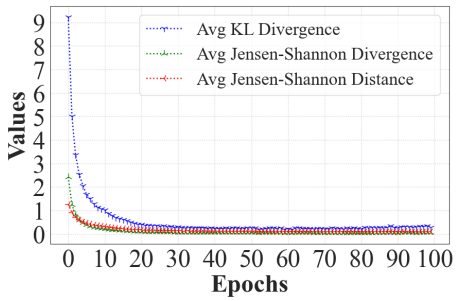

Figure 5: Domain adaptation distance and divergence metrics over epochs.

all categories, with 98% accuracy for clean EEG segments. Among artifacts, Eye Movement and Muscle achieved accuracies of 92% and 91%, respectively, while Chewing and Shiver reached 88% and Electrode Pop 82%.

Despite the overall strong performance, off-diagonal entries reveal confusion mainly between Chewing and Muscle artifacts and between Electrode Pop and Eye Movement, reflecting their spectral and temporal similarities. The dominant diagonal entries confirm that the model effectively discriminates physiological and non-physiological artifacts in both real and synthetic EEG data, supporting its suitability for automated artifact detection and EEG preprocessing pipelines.

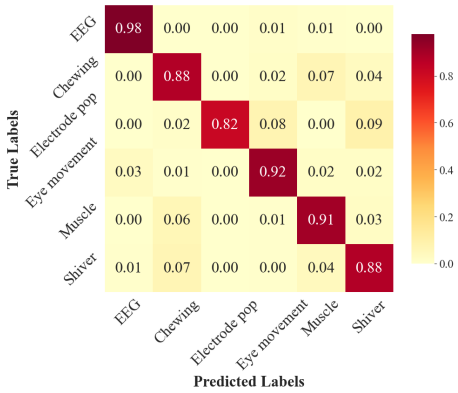

Figure 6: Confusion matrix — Source and Target domains.

Table 2 highlights clear differences in class-wise behavior between the TUH-EEG and EEGdenoiseNet Custom domains. Overall, the DA-NN model maintains strong discrimination for clean EEG activity across both datasets, indicating stable separation between artifact-free and contaminated signals. For most artifact classes, EEGdenoiseNet Custom exhibits equal or improved performance relative to TUH-EEG, suggesting that the domain-adaptation strategy effectively leverages the more controlled structure of the synthetic data. This improvement is particularly evident for muscle artifacts, where the model benefits from the higher consistency and signal-to-noise control inherent to EEGdenoiseNet, leading to more reliable feature learning.

In contrast, electrode pop artifacts show reduced performance in the synthetic domain, likely reflecting the difficulty of accurately modeling abrupt, non-physiological disturbances using synthetic generation procedures. Smaller yet consistent gains are observed for chewing, eye movement, and shiver artifacts, indicating that the adaptation mechanism improves generalization without overfitting to domain-specific characteristics. Overall, these results demonstrate that the proposed DA-NN balances robustness and sensitivity across heterogeneous domains, while also revealing artifact types for which synthetic data remain less representative of real-world EEG conditions.

5.4 Discussion of Results

While Table 3 reports overall accuracy as the primary metric, comparison with additional measures in the literature reveals clear differences in robustness that favor the proposed DA-NN. Prior works achieve their reported accuracies under substantially different trade-offs between sensitivity, specificity, and class balance.

The baseline method of Kim and Keene (Kim and Keene, 2019) reports an accuracy of 67.59% with a true positive rate of approximately 80% for binary artifact detection, but at the cost of a high false alarm rate of 25.82%. In contrast, the proposed DA-NN increases accuracy to 91.59% while achieving consistently higher specificity across all artifact classes (Table 2), indicating that performance gains are driven by reduced false positives rather than aggressive detection.

The Transformer-based approach of Peh et al. (Peh et al., 2022) achieves an intermediate accuracy of 79.22%, with balanced accuracy values ranging from 0.655 to 0.947. However, their binary detector exhibits sensitivities between 35.3% and 60.4% at high-specificity operating points (95–99%), reflecting a strong sensitivity–specificity trade-off. By contrast, the DA-NN maintains high sensitivity and specificity simultaneously; for example, ocular and muscle artifacts in the target domain achieve F1-scores of 0.9468 and 0.9554, with specificities above 0.99.

Image-based time–frequency methods, such as the spectrogram-based approach of Maiwald et al. (Maiwald et al., 2023), report accuracies up to

Table 2: Comparison of classification performance metrics per class between TUH-EEG and EEGdenoiseNet Custom.

Class	TUH-EEG				EEGdenoiseNet Custom			
	Precision	**Sensitivity**	**F1-score**	**Specificity**	**Precision**	**Sensitivity**	**F1-score**	**Specificity**
EEG	0.9896	0.9566	0.9728	0.9972	0.9325	1.0000	0.9651	0.9795
Chewing	0.8878	0.8440	0.8654	0.9709	0.8999	0.9071	0.9035	0.9724
Electrode pop	1.0000	0.8485	0.9180	1.0000	0.7879	0.7879	0.7879	0.9983
Eye movement	0.9449	0.9255	0.9351	0.9841	0.9727	0.9222	0.9468	0.9923
Muscle	0.8116	0.8814	0.8450	0.9451	0.9769	0.9349	0.9554	0.9941
Shiver	0.8350	0.8755	0.8548	0.9772	0.8563	0.8797	0.8678	0.9805

Table 3: Comparison of the proposed method versus state-of-the-art approaches

Method	**Feature Type**	**Accuracy**
(Kim and Keene, 2019)	Baseline EEG	67.59%
(Peh et al., 2022)	Baseline EEG statistics	79.22%
(Maiwald et al., 2023)	Spectrogram	88.30%
DA-NN model	**STFT magnitude**	**91.59%**

88.30% and F1-scores near 0.90 in single-domain evaluations. The DA-NN exceeds this accuracy while preserving high precision and recall across both TUH-EEG and EEGdenoiseNet Custom, demonstrating improved robustness under domain shift.

Overall, when accuracy is taken as a reference, the proposed DA-NN outperforms prior methods not only in overall correctness but also in clinically relevant metrics, including sensitivity, specificity, balanced accuracy, and F1-score, providing a more stable trade-off across all measures.

6 CONCLUSIONS

In conclusion, this study proposed the DA-NN model, a semi-supervised domain-adaptation approach for EEG artifact classification. The Sinkhorn-based alignment strategy proved effective on both real and synthetic EEG data, improving robustness under distributional shifts. Training on a real-data source domain enabled accurate identification of multiple artifact types, while incorporating a target domain with controlled SNR variations enhanced generalization under adverse conditions, yielding an overall accuracy of 91.59%. Notably, the proposed DA-NN reduced the performance gap between real and synthetic domains by 24%, highlighting the effectiveness of domain adaptation for cross-domain EEG analysis. Future work will explore fully unsupervised learning using real unlabeled EEG recordings, aiming to remove dependence on labeled datasets while maintaining competitive classification performance.

REFERENCES

Ahmed, A. (2022). A quick survey of eeg signal noise removal methods. *Global Journal of Engineering and Technology Advances*, 11:098–104.

Bahador, N., Erikson, K., Laurila, J., Koskenkari, J., Ala-Kokko, T., and Kortelainen, J. (2020). Automatic detection of artifacts in eeg by combining deep learning and histogram contour processing. In *2020 42nd Annual International Conference of the IEEE Engineering in Medicine & Biology Society (EMBC)*, pages 138–141.

Cai, Y., Meng, Z., and Huang, D. (2025). Dhct-gan: Improving eeg signal quality with a dual-branch hybrid cnn–transformer network. *Sensors*, 25(1).

Choi, B. J. (2025). Removing neural signal artifacts with autoencoder-targeted adversarial transformers (at-at).

Chuang, C.-H., Chang, K.-Y., Huang, C.-S., and Jung, T.-P. (2022). Ic-u-net: A u-net-based denoising autoencoder using mixtures of independent components for automatic eeg artifact removal. *NeuroImage*, 263:119586. Epub ahead of print, August 27, 2022.

Courty, N., Flamary, R., Habrard, A., and Rakotomamonjy, A. (2017a). Joint distribution optimal transportation for domain adaptation. In *Proceedings of the 31st International Conference on Neural Information Processing Systems*, NIPS'17, page 3733–3742, Red Hook, NY, USA. Curran Associates Inc.

Courty, N., Flamary, R., Tuia, D., and Rakotomamonjy, A. (2017b). Optimal transport for domain adaptation. *IEEE Transactions on Pattern Analysis and Machine Intelligence*, 39(9):1853–1865.

Farahani, A., Voghoei, S., Rasheed, K., and Arabnia, H. R. (2021). A brief review of domain adaptation. In Stahlbock, R., Weiss, G. M., Abou-Nasr, M., Yang, C.-Y., Arabnia, H. R., and Deligiannidis, L., editors, *Advances in Data Science and Information Engineering*, pages 877–894, Cham. Springer International Publishing.

Feydy, J., Séjourné, T., Vialard, F.-X., Amari, S.-i., Trouve, A., and Peyré, G. (2019). Interpolating between optimal transport and mmd using sinkhorn

divergences. In *The 22nd International Conference on Artificial Intelligence and Statistics*, pages 2681–2690.

Fuglede, B. and Topsoe, F. (2004). Jensen-shannon divergence and hilbert space embedding. In *International Symposium onInformation Theory, 2004. ISIT 2004. Proceedings.*, pages 31–.

Géron, A. (2019). *Hands-On Machine Learning with Scikit-Learn, Keras, and TensorFlow: Concepts, Tools, and Techniques to Build Intelligent Systems*. O'Reilly Media, 2nd edition.

Geuter, J., Kornhardt, G., Tomasson, I., and Laschos, V. (2025). Universal neural optimal transport. In Singh, A., Fazel, M., Hsu, D., Lacoste-Julien, S., Berkenkamp, F., Maharaj, T., Wagstaff, K., and Zhu, J., editors, *Proceedings of the 42nd International Conference on Machine Learning*, volume 267 of *Proceedings of Machine Learning Research*, pages 19196–19232. PMLR.

Goyal, D. and Pabla, B. (2015). Condition based maintenance of machine tools—a review. *CIRP Journal of Manufacturing Science and Technology*, 10:24–35.

Grandini, M., Bagli, E., and Visani, G. (2020). Metrics for multi-class classification: an overview. *ArXiv*, abs/2008.05756.

Hamid, A., Gagliano, K., Rahman, S., Tulin, N., Tchiong, V., Obeid, I., and Picone, J. (2020). The temple university artifact corpus: An annotated corpus of eeg artifacts. In *2020 IEEE Signal Processing in Medicine and Biology Symposium (SPMB)*, pages 1–4.

Huang, X., Li, C., Liu, A., Qian, R., and Chen, X. (2024). Eegdfus: A conditional diffusion model for fine-grained eeg denoising. *IEEE Journal of Biomedical and Health Informatics*, pages 1–13.

Jackson, A. F. and Bolger, D. J. (2014). The neurophysiological bases of eeg and eeg measurement: a review for the rest of us. *Psychophysiology*, 51(11):1061–1071. Epub 2014 Jul 17.

Kim, D. and Keene, S. (2019). Fast automatic artifact annotator for eeg signals using deep learning. In *2019 IEEE Signal Processing in Medicine and Biology Symposium (SPMB)*, pages 1–5.

Lin, H.-Y., Tseng, H.-H., Lu, X., and Tsao, Y. (2021). Unsupervised noise adaptive speech enhancement by discriminator-constrained optimal transport.

Maiwald, A., Ackermann, L., Kalcher, M., and Wu, D. J. (2023). Image-based data representations of time series: A comparative analysis in eeg artifact detection.

Mashhadi, N., Khuzani, A. Z., Heidari, M., and Khaledyan, D. (2020). Deep learning denoising for eog artifacts removal from eeg signals. *2020 IEEE Global Humanitarian Technology Conference (GHTC)*, pages 1–6.

Peh, W. Y., Yao, Y., and Dauwels, J. (2022). Transformer convolutional neural networks for automated artifact detection in scalp eeg. *2022 44th Annual International Conference of the IEEE Engineering in Medicine & Biology Society (EMBC)*, pages 3599–3602.

Quintero-Rincón, A., Giano, C. D., and Batatia, H. (2021). Chapter 11. artefacts detection in eeg signals. In *Artefacts Detection in EEG Signals*.

Saba-Sadiya, S., Chantland, E., Alhanai, T., Liu, T., and Ghassemi, M. M. (2021). Unsupervised eeg artifact detection and correction. *Frontiers in Digital Health*, 2.

Shlens, J. (2014). Notes on kullback-leibler divergence and likelihood. *ArXiv*, abs/1404.2000.

Tohka, J. and van Gils, M. (2021). Evaluation of machine learning algorithms for health and wellness applications: A tutorial. *Computers in Biology and Medicine*, 132:104324.

Zhang, H., Zhao, M., Wei, C., Mantini, D., Li, Z., and Liu, Q. (2021). Eegdenoisenet: a benchmark dataset for deep learning solutions of eeg denoising. *Journal of Neural Engineering*, 18(5):056057.

Zunino, L., Olivares, F., Ribeiro, H. V., and Rosso, O. A. (2022). Permutation jensen-shannon distance: A versatile and fast symbolic tool for complex time-series analysis. *Phys. Rev. E*, 105:045310.